UC Santa Cruz

UC Santa Cruz Electronic Theses and Dissertations

Title

Annealing Induced Transmission Improvements and Photoluminescence Reduction of ARROW Optofluidic Chips for Improved Fluorescence Detection

Permalink

https://escholarship.org/uc/item/25v901x9

Author

Parks, Joshua W.

Publication Date

2012

Peer reviewed|Thesis/dissertation

UNIVERSITY OF CALIFORNIA

SANTA CRUZ

**Annealing Induced Transmission Improvements and Photoluminescence
Reduction of ARROW Optofluidic Chips for Improved Fluorescence Detection**

A thesis submitted in partial satisfaction
Of the requirements for the degree of

MASTER OF SCIENCE

in

CHEMISTRY

by

Joshua W. Parks

December 2012

The Thesis of Joshua W. Parks is approved:

_____
Professor Jin Zhang, Chair

_____
Professor Holger Schmidt

_____
Professor Michael Stone

_____
Tyrus Miller
Vice Provost and Dean of Graduate Studies

List of Figures

Abstract

Joshua W. Parks

Annealing Induced Transmission Improvements and Photoluminescence

Reduction of ARROW Optofluidic Chips for Improved Fluorescence Detection

Effects of thermal annealing on liquid- and solid-core antiresonant reflective optical waveguides (ARROW) are herein investigated. Transmission changes of 10 to 1000 fold increases are observed post annealing at either 300 or 700 °C. Furthermore, upon 700 °C annealing, the detectable photoluminescence of tantalum oxide cladding layers is reduced to half that of its original value. The suggestible cause for change in transmission is increased modal confinement within the ridge waveguides. Although annealing cracks form at all temperatures, their effect on transmission seems intermittent. A final culmination of the transmission changes is observed in a protein detection experiment where a 6.3 fold signal increase is observed after annealing.

Introduction

Optofluidics has becoming a flourishing field in the past decade due to its promising contributions in current biosensing. One way of probing fluids is through the use of traditional waveguides based on total internal reflection (TIR). In most cases, the implementation of this principle means that biosensors must rely on evanescent fields for sensing.[1,2,3] The low mode-analyte spatial overlap means that non-dramatic fluctuations will induce only slight changes in readout. Although a few inventive TIR guiding sensors have achieved high mode-analyte overlaps, their implementation remains challenging due to constraints such as low mode volume[4] and instability of structures.[5]

Non-conventional guiding provides another means of creating modal confinement in low index media. More specifically, interference phenomena can be used to confine originally leaky modes.[6] Utilizing these principles, the Schmidt group has created a next generation planar optofluidic platform implementing antiresonant reflecting optical waveguides (ARROWs). Using these structures, we have been able to show fluorescence detection of single fluorescent molecules,[7] particles,[8] and viruses.[9] As these experiments relied heavily on fluorescence detection technology, three natural limitations arose for the ARROW platform: incomplete filtering of excitation light, spurious background signal, and incomplete signal collection. Our group has worked to overcome these challenges through a variety of methods. In the

case of excitation filtering, on chip static and tunable filters were created for exclusion of unwanted signal.[10,11] Reduction of spurious signal was achieved through proper choice of ARROW cladding layers in which photoluminescence was minimized.[12] Finally, multiple improvements have been made to the ARROW structure in order to improve optical transmission yielding approximately 2-17 fold improvements.[13,14,15,16] However, total optical transmission for a given ARROW chip—all improvements accounted for—was still on average about 1%.

Here, we present a completely new way of both reducing spurious signal and increase optical transmission with dramatic effects. Through thermal annealing of optofluidic ARROW waveguides, liquid core broadband transmission increases 10-1000 fold and waveguide photoluminescence is reduced to a level comparable to detector background. Optofluidic chips with throughputs upwards of 30% are observed. It is also shown that these improvements translate directly to increased signal to noise in fluorescence measurements. The mechanism of transmission increase is suggested to be improved modal confinement possibly due to reduction of top oxide hydration.

Materials and Methods

Fabrication: Thin films and hollow core ARROW layers were grown using Plasma Enhanced Chemical Vapor Deposition. In the case of hollow core samples, Evaporative Coatings Inc. grew ARROW layers with the following structure, thicknesses (in microns), and indexes (at 632.8 nm) – $Si/SiO_2/Ta_2O_5/ SiO_2/Ta_2O_5/ SiO_2/Ta_2O_5$, 500/0.265/0.102/0.265/0.102/0.265/0.102, and 3.85/1.47/2.107/1.47/2.107/1.47/2.107. Fabrication of the waveguide structures followed established single over coating (SOC) and self-aligned pedestal (SAP) techniques and was carried out at Brigham Young University by the Hawkins
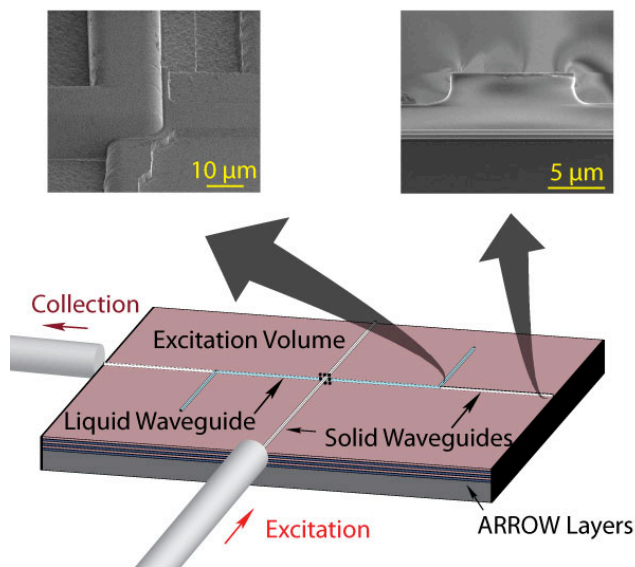

Figure 1 – Optofluidic ARROW chip layout in a typical detection scenario. Note that SEM images indicate the collection-solid-core waveguide interface (left) and collection solid-core waveguide facet (right).

Group.[14,15] Excitation solid core waveguides are 4x4 μm (width x height), while collection solid core and the liquid core waveguides are 12x5 μm. Figure 1 shows the overall chip layout in a typical fluorescence detection scenario.

Annealing: Tantalum oxide thin films were rapidly annealed at respective temperatures for 30 minutes in air or nitrogen (both environments exhibiting similar results). Liquid and solid core waveguides were annealed in either a Lindberg/Blue M Tube or Box furnace. The Temperature profile for annealing at 300 °C was designed as follows: 25 °C to 300 °C (ramp rate 2.5 °C/min), 300 °C constant temperature (10 hours), 300 °C to 25 °C (ramp rate –2.5 °C/min). Similarly, the 700 °C annealing was conducted with the following parameters: 25 °C to 700 °C (ramp rate 2.5 °C/min), 700 °C constant temperature (30 minutes), 700 °C to 25 °C (ramp rate –2.5 °C/min). Shorter peak temperature annealing in the 700 °C experiment was used to compensate for the long ramp time. It is notable, however, that ramp rate and peak temperature annealing time had little effect on outcome.

Loss Simulations: Analytical 2x2 matrix formalism calculations were used to simulated liquid and solid core loss.[17,18] The index of the guiding and ARROW layers were presumed to be constant over the simulated range of wavelengths. Transmission spectra were generated using the following formula $P_o/P_i = e^{-(\alpha_{LC}(\lambda)+\alpha_{SC}(\lambda))*l}$, where l was taken to be 4 mm and the wavelength (λ) dependence of the solid and liquid core waveguide loss (α) was made explicit. Also note that surface roughness was not taken into account.

4

Sample Transmission Spectra: Sample transmission spectra were taken using a home-built femtosecond laser-photonic crystal fiber white light source.[10,11] As the output of such a source is relatively un-polarized, transmission characteristics for x (horizontal) and y (vertical) polarization were measured using a polarization analyzer implemented between the Optical Spectrum Analyzer (OSA) and optofluidic chip. Both liquid and solid core transmission spectra were obtained with a Phosphate Buffered Saline (PBS) filled hollow core. Solid core measurements refer to light passing through the entire excitation solid core (and 12 μm width of the liquid core). Liquid core measurements denote passing longitudinally through collection solid core, liquid core, and back out the opposing collection solid core. X-polarization denotes an input of horizontal orientation, when the optofluidic features are facing up.

Mode Imaging: HeNe laser light was passed (via a single mode fiber) through the collection solid cores and liquid core onto a mode-imaging (CCD) camera. The output of the camera was recorded using a Beam PROfiler (Photon Inc.).

Ellipsometry Measurements: Ellipsometry measurements of thin films were performed on a Rudolph AutoEL Automatic Ellipsometer at 632.8 nm. Each datum is an average of 3-5 measurements. Thicknesses measurements were confirmed via scanning electron microscopy.

Photoluminescence and Fluorescence Detection: Background photoluminescence and fluorescent molecule detection were performed in a detection scheme similar to that previously reported.[12] A Melles Griot 632.8 nm HeNe laser was used for excitation in all experiments and was introduced via a single mode fiber. Orthogonal

collection of signal was achieved through a 40x objective, after which it was passed

through a 40 nm band-pass filter centered at 670 nm. The signal was then coupled

into a multimode fiber and finally detected using a Single Photon Avalanche

Photodiode (SPAPD) in conjunction with a Time Correlated Single Photon Counting

(TCSPC) TimeHarp card. PBS was used to fill ARROW samples during background

performance tests, as fluorescent molecules in later experiments were solvated in this

buffer. Note that all solutions contained a baseline concentration of 0.1x Bovine

Serum Albumin (BSA) used as a dynamic surface passivation technique to prevent

analyte-wall binding during fluorescence measurements.[19] BSA caused no detectable

change in background or throughput.

Results and Discussion

Direct characterization of sample throughput before and after 700 °C annealing is presented in Figure 2. Included for clarity are improvement factor vs. wavelength graphs which depict the ratio of power throughput before and after annealing. It is clear that in both the case of solid core and liquid core measurements that the transmission is dramatically increased. Furthermore, this statement holds for both x and y-polarizations. As noted for the x-polarized solid core transmission, a
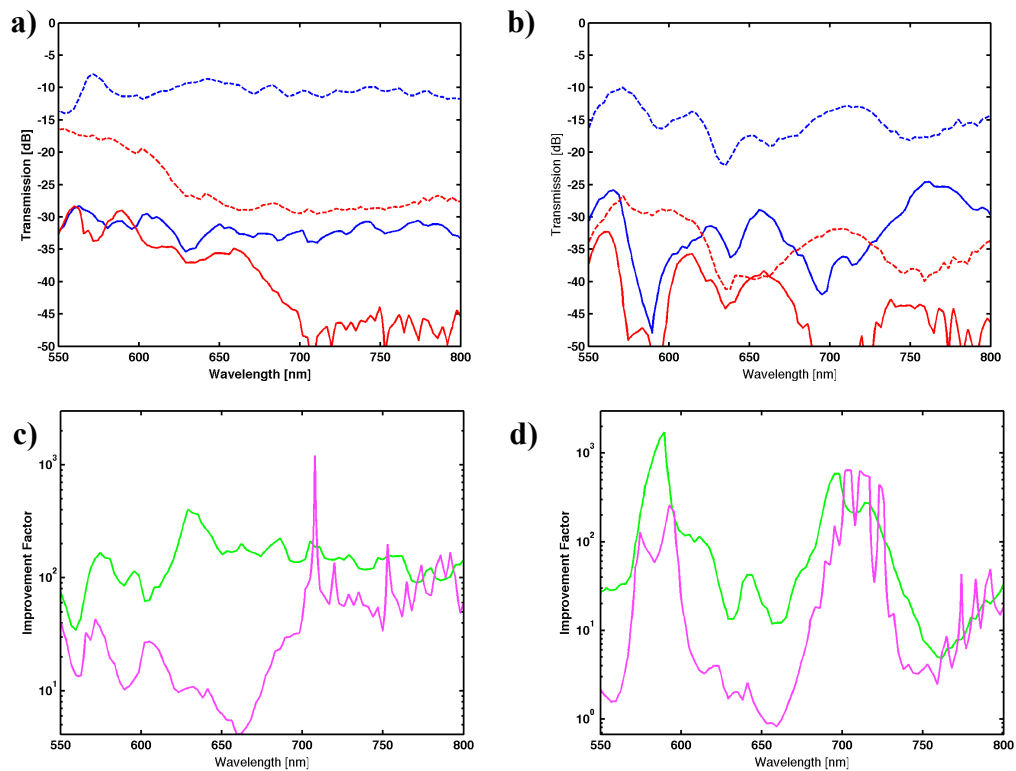
Figure 2 - Solid **(a)** and liquid **(b)** core white light transmission spectra. Pre-annealing measurements are solid lines and post-annealing measurements are dashed lines. X and Y-polarizations are denoted by blue and red respectively. The improvement factor of transmission is plotted in **(c)** and **(d)** for solid and liquid core waveguides respectively. Here, y-polarization improvement is in magenta where x-polarization improvement is in green.

broadband increase in transmission of on average 20 dB—or a 100-fold improvement

of power transmission—was observed. This result was confirmed using a single

wavelength 632.8 nm HeNe yielding a percent transmission (%T) change from 0.25

to 30%. The latter value is a power transmission three times higher than the best

ARROW chip ever created (of which there was only one). However, such

transmission changes were not limited to solid cores. As seen in Figure 1(b), the

liquid core transmission dramatically changed for x-polarization as well. In fact, other

liquid core chips experienced over 300x increase in %T for x-polarized input light. It

is not unexpected that the y-polarized liquid core transmission did not experience as

much of a change as this input polarization couples into a far "leakier" (higher loss)

mode and is theoretically limited to a transmission of 10-50 dB lower than that of x-

polarized light for the current design. Note that the leakier nature of the y-polarized

mode is due to the Transverse Magnetic (TM) boundary conditions imposed by the

silicon-ARROW layer structure. However, it is apparent in Figure 2 (d) that some

wavelengths did also experience dramatic improvements (over 100 fold) for y-

polarization guiding.

As these waveguides are inherently lossy and are essentially based on the

reflectivity of ARROW layers, the loss has a dependence on wavelength. As such, it

becomes important to account for deviations in ARROW layer properties. More

specifically, it is important to consider the change in refractive index and thickness of

tantalum oxide films upon annealing. Ellipsometry measurements on 150 nm thin

films were conducted yielding the data presented in Figure 3. Notable changes in both

8

refractive index and thickness are apparent for all annealing temperatures in comparison to as grown (250 °C) samples. The change in refractive index and thickness are far larger for samples annealed at 700 °C in comparison to 300 °C
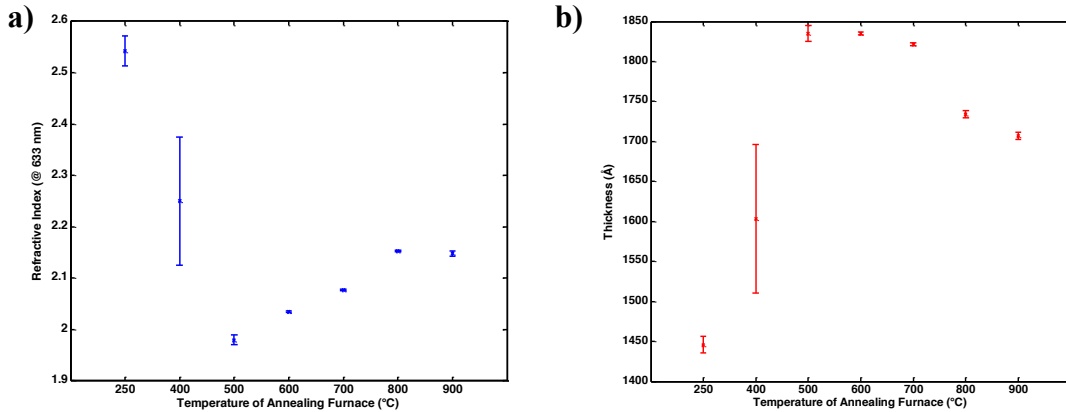

Figure 3 - (a) Refractive index and **(b)** thicknesses measurements of tantalum oxide thin films at 633 nm at various post processing annealing temperatures. Each point is an average of 3-5 measurements, from which the error bars were generated.

(interpolated) and were thus considered for their effects on ARROW guiding.

Considering the ratio of refractive index (n_{250} / n_{700}) and thickness (t_{250} / t_{700}), transmission simulations were performed concerning the designed thicknesses and indexes. Figure 4 displays the thin film predicted changes in transmission. It is clear that the transmission is dramatically reduced for all wavelengths (less 725-800 nm for y-polarized light) when refractive indexes and thicknesses of ARROW tantalum oxide layers are altered according to Figure 3. This is not unexpected as ARROW
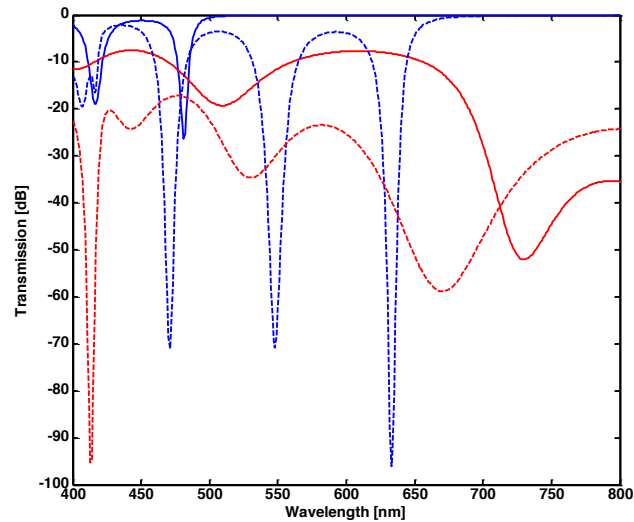
Figure 4 - Transmission simulations for design and "thin film predicted" structures. X-polarization is presented in blue and y-polarization is presented in red. The designed structure transmissions are solid lines, whereas dashed lines indicate the "thin film predicted" annealing structures (n_{250} / n_{700} and t_{250} / t_{700} accounted for).

layers are designed to be optimally transmissive around 633 nm which is in direct

contrast to measured results. In other words, simulations of expected thin film index

and thickness changes suggest an increase in loss (decrease in transmission) due to

annealing, where the actuality is that transmission is increased. Thus, it is concluded

that thin film expansion and refractive index changes cannot account for the increased

transmission of annealed ARROW chips. Note also that significant changes in layer

thickness were not observed upon SEM imaging – validating this conclusion.

Although further studies will be conducted on index and thickness changes of silicon

dioxide films, it is suspected that changes (if any) will only decrease theoretical

transmission of samples.

Another aspect of the chip that could change during annealing is the thick top oxide. As it is porous, it can fairly readily incorporate water. Such incorporation can
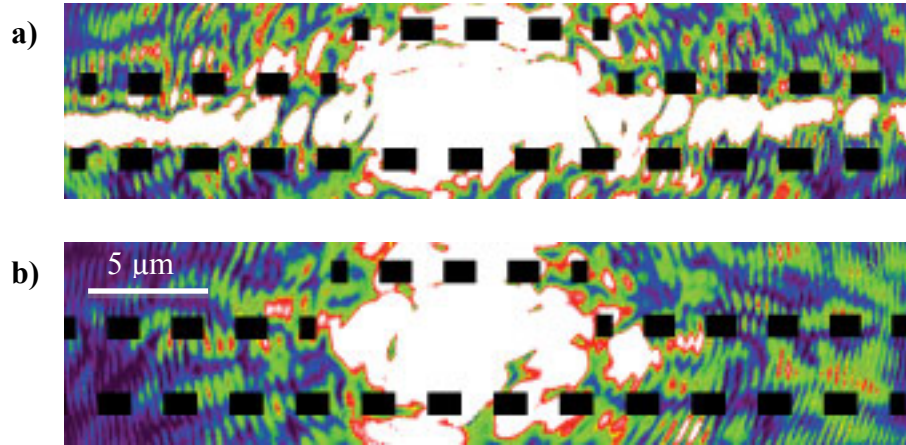
Figure 6 – Mode images of **(a)** pre- and **(b)** post-annealing liquid-collection solid cores. High intensity (white) is apparent throughout the top oxide (indicated by dashed lines – see **Figure 1** inset for example profile) pre-annealing and is confined within the core post-annealing.

Figure 6 - Time dependence of liquid core ARROW transmission stored in different partial pressures of water. The colors black, blue, and red represent desiccator, room, and high partial pressures of water respectively.

11

cause average index changes, thereby altering the guiding properties. The possibility of top oxide changes was investigated through 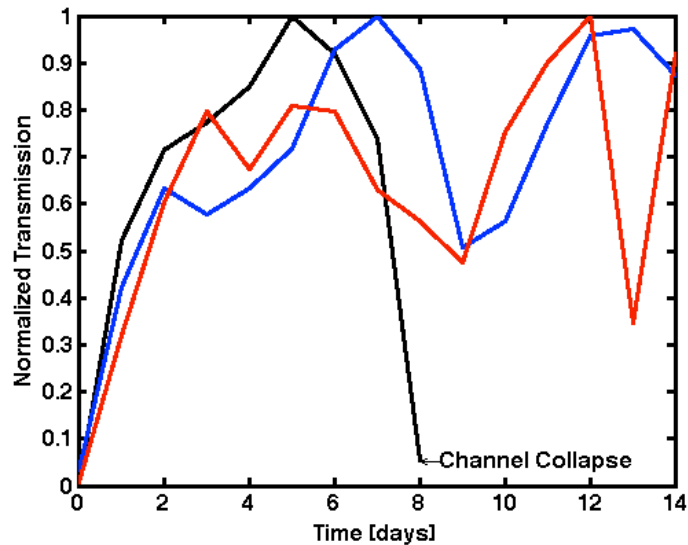mode imaging (because changes in index would affect modal confinement). The output modes of a sample pre- and post-annealing are presented in Figure 6. It is clearly evident that the lateral confinement is much better after annealing than before. It is important to realize that this lateral confinement is important for both liquid core throughput and fluorescence measurements. In the case of throughput, the light leaking into the sides of the top oxide will not couple into the liquid core and will be lost at the "intersection". Considering fluorescence detection, an iris is used to exclude scattered and photoluminescence outside the collection solid core facet. Thus, any signal that has leaked outside of the core will be lost before reaching the detector. Although variations in surface roughness of top oxide (due to annealing) could be considered as a means of transmission improvement, atomic force microscopy (AFM) measurements disprove this hypothesis.

  With varying oxide hydration being a possible cause of transmission increases, waveguide transmission dependence on ambient moisture was also tested. For this test, waveguides were stored in three conditions: 1) within a desiccator, 2) at room partial pressure of water, and 3) high partial pressure of water created by storing ARROW samples in a clean beaker surrounded by water (and covered by a petri dish). Respective results are presented Figure 6 where time 0 indicates pre-annealing transmission. The first notable aspect of this plot is the initial value for the transmissions. In every case, the pre-annealing samples had transmissions lower than

5% of their respective maximum. Also, it is clear the transmission is a function of time. However, there seems to be no correlation between ambient moisture and normalized transmission. The channel collapse of the desiccated sample was likely due to a structural irregularity and is not attributed to either the annealing or desiccation process. An oscillatory nature of the transmission is present in each of the un-collapsed samples and indicates that the cause of temporal transmission dependence is reversible.
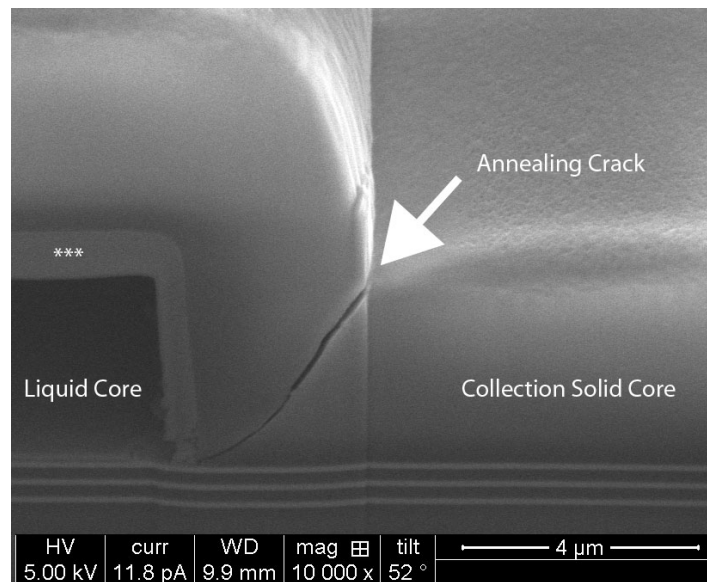

Figure 7 – SEM image of liquid core-collection solid core intersection and aberrant annealing crack. *** Indicates a curtaining layer apparent as an artifact of Focused Ion Beam (FIB) cross sectioning.

It is speculated that the cause of transmission fluctuations arises from a byproduct of annealing. More specifically, upon annealing, the thick top oxide of the sample experiences stress due to dehydration.[20,21] This stress causes cracking at structurally weak positions of the chip. One such point is present at the collection solid core-liquid core intersection. Appearing in Figure 7, the crack at the intersection

is approximately at 45° and lies directly in the optical path. If filled with water, the index of the crack would be approximately 1.33. However, if unfilled, the crack has an index equivalent to air (1.0). Consequently, it can be hypothesized that upon incomplete hydration of the crack, transmission would actually decrease as an artifact of annealing due to scattering at the silicon dioxide air boundary. On the contrary, if filled with water, the index matching could be close enough to alleviate any dramatic scattering effects caused by the crack. Thus, it is postulated that fluctuations in throughput correspond to different amounts of water in the crack, where a completely filled crack represents the highest throughput. Consequently, for longevity and consistency, research is still being conducted on a means to keep the annealing cracks from forming altogether.
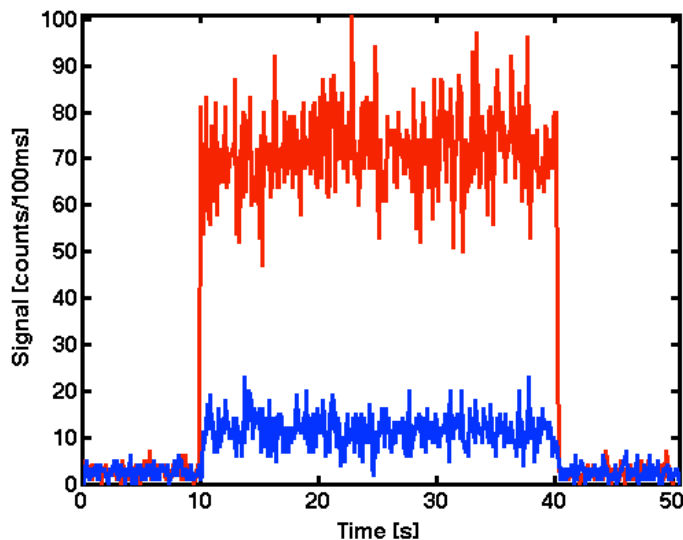

Figure 8 – Fluorescence detection of Dylight 633 coupled 100 pM Goat anti-Rabbit antibody. Detection was conducted separately on annealed and un-annealed ARROW optofluidic chips presented in red and blue respectively.

14

Cracks notwithstanding, the transmission increase in annealed samples also guides the internally generated light of fluorescence better. Exhibited in Figure 2 (b), the transmission for 633 nm and 660 nm increased for both x- and y-polarizations upon annealing. These wavelengths correspond to excitation and emission lines of Dylight 633. As a proof of principle, Dylight 633 coupled Goat anti-Rabbit antibody was detected in an un-annealed (5% liquid core throughput) and annealed (30% liquid core throughput) ARROW chip at 100 pM protein concentration (at ~3 dye/protein).

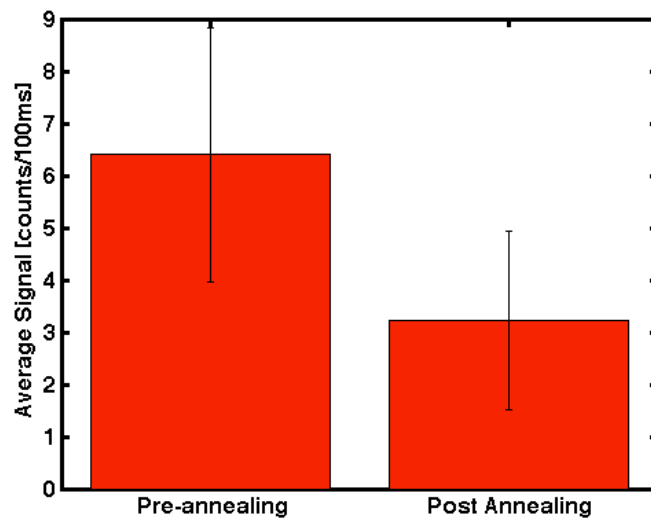**Figure 9 –** Orthogonally collected background photoluminescence from ARROW layers.

Background subtracted fluorescence signal appears between 10 and 40 seconds in Figure 8. During the first and last ten seconds the excitation laser is turned off. A 6.3 fold change in average fluorescence signal is in excellent agreement with the transmission change in the sample. Fluctuations in signal are attributed to coupling changes.

Better guiding of signals (less loss) is one way to improve signal to noise –
another is to reduce background. The orthogonally collected background (generated
via ARROW layer photoluminscence[12]) was tested on a sample pre and post-
annealing. The results are presented in Figure 9. Background reduction upon
annealing at 700 °C is twofold and reduces background signal to only three photons
per 100 ms. In Figure 9, error bars represent the fluctuation in photoluminescence
signal. Spurious signal was not reduced for 300 °C annealed samples, supporting
previous findings.[22] Another notable point is that the higher temperature (700 °C)
increased the amount of stress experienced by samples and subsequently increased
the amount of cracking such as that seen in Figure 6. Thus, it is advisable to anneal
deposited ARROW layers before chip production so as to reduce background while
minimizing cracking.

Conclusions and Future Work

We have above described the effects of thermal annealing on the performance of optofluidic ARROW waveguide devices, specifically on waveguide throughput and generation of spurious background fluorescence. More specifically, the transmission for both solid- and liquid-core waveguides improved dramatically upon 300 and 700 °C annealing. Changes in liquid- and solid-core waveguide throughput were 10 to 1000 fold for x-polarization light while the solid-core waveguides also experienced similar improvements for y-polarization. Although change in transmission seems to be irrespective of annealing temperature (300 vs. 700 °C), photoluminescence was only reduced in the case of high temperature annealing. It is notable that this decrease in spurious signal came at the cost of top oxide cracking in most cases. Loss simulations suggest that the increase in transmission is not due to thermal expansion or index changes in tantalum oxide cladding layers. Rather, the changes seem to be caused by increased modal confinement due to elimination of water. To this end, further studies need to be conducted on index and thickness properties of silicon dioxide thin films at various annealing temperatures. Also, retaining a filled sample over the course of a week could rule out (or support) annealing cracks as the cause of transmission fluctuations. The work herein provides a means for increasing throughput of ARROW devices for sensitive detection of single molecules.

Bibliography

(1)   Vollmer, F.; Braun, D.; Libchaber, a.; Khoshsima, M.; Teraoka, I.; Arnold, S. *Applied Physics Letters* **2002**, 80, 4057.

(2)   Suter, J. D.; White, I. M.; Zhu, H.; Shi, H.; Caldwell, C. W.; Fan, X. *Biosensors and Bioelectronics* **2008**, 23, 1003–1009.

(3)   Levene, M. J.; Korlach, J.; Turner, S. W.; Foquet, M.; Craighead, H. G.; Webb, W. W. *Science (New York, N.Y.)* **2003**, 299, 682–6.

(4)   Barrios, C. A.; Bañuls, M. J.; González-Pedro, V.; Gylfason, K. B.; Sánchez, B.; Griol, A.; Maquieira, A.; Sohlström, H.; Holgado, M.; Casquel, R. *Optics Letters* **2008**, 33, 708.

(5)   Risk, W.; Kim, H.; Miller, R.; Temkin, H.; Gangopadhyay, S. *Optics express* **2004**, 12, 6446–55.

(6)   Duguay, M.; Kokubun, Y.; Koch, T.; Pfeiffer, L. *Applied Physics Letters* **1986**, 49, 13–15.

(7)   Yin, D.; Deamer, D. W.; Schmidt, H.; Barber, J. P.; Hawkins, A. R. *Optics letters* **2006**, 31, 2136–8.

(8)   Yin, D.; Lunt, E. J.; Rudenko, M. I.; Deamer, D. W.; Hawkins, A. R.; Schmidt, H. *Lab on a chip* **2007**, 7, 1171–5.

(9)   Rudenko, M. I.; Kühn, S.; Lunt, E. J.; Deamer, D. W.; Hawkins, a R.; Schmidt, H. *Biosensors & bioelectronics* **2009**, 24, 3258–63.

(10)   Measor, P.; Phillips, B. S.; Chen, A.; Hawkins, A. R.; Schmidt, H. *Lab on a chip* **2011**, 11, 899–904.

(11)   Ozcelik, D.; Phillips, B. S.; Parks, J. W.; Measor, P.; Gulbransen, D.; Hawkins, A. R.; Schmidt, H. *Lab on a chip* **2012**, 12, 3728–33.

(12)   Zhao, Y.; Jenkins, M.; Measor, P.; Leake, K.; Liu, S.; Schmidt, H.; Hawkins, a R. *Applied physics letters* **2011**, 98, 91104.

(13)   Yin, D.; Barber, J.; Hawkins, A.; Schmidt, H. *Optics express* **2005**, 13, 9331–6.

(14) Lunt, E. J.; Wu, B.; Keeley, J. M.; Measor, P.; Schmidt, H.; Hawkins, A. R. *IEEE photonics technology letters : a publication of the IEEE Laser and Electro-optics Society* **2010**, 22, 1147–1149.

(15) Lunt, E. J.; Measor, P.; Phillips, B. S.; Kühn, S.; Schmidt, H.; Hawkins, A. R. *Optics express* **2008**, 16, 20981–6.

(16) Zhao, Y.; Leake, K.; Measor, P.; Jenkins, M.; Keeley, J. *Photonics Technology Letters* **2012**, 24, 46–48.

(17) Yeh, P. *Optical waves in layered media*; John Wiley & Sons Inc.: Hoboken, NJ, 1998.

(18) Archambault, J.-L.; Black, R. J.; Lacroix, S.; Bures, J. *Journal of Lightwave Technology* **1993**, 11, 416–423.

(19) Zhang, C.; Xu, J.; Ma, W.; Zheng, W. *Biotechnology advances* **2006**, 24, 243–84.

(20) Adams, A. C.; Alexander, F. B.; Smith, C. D.; Capio, T. E. *Journal of The Electrochemical Society* **1981**, 128, 1545.

(21) Haque, M. S.; Naseem, H. a.; Brown, W. D. *Journal of Applied Physics* **1997**, 82, 2922.

(22) Zhao, Y.; Phillips, B.; Ozcelik, D.; Parks, J.; Measor, P.; Gulbransen, D.; Schmidt, H.; Hawkins, A. R. *Journal of biophotonics* **2012**, 9, 1–9.